Resource Allocation for Joint Communication and Positioning in mmWave Ad hoc Networks

Xueni Luo, Xiaofeng Lu, Benquan Yin, and Kun Yang, *Follow, IEEE*

***Abstract*—Joint communication and positioning will be a critical driver in future wireless networks for emerging application areas. Supporting mobility, Ad-hoc networks can freely and dynamically self-organize an arbitrary and temporary network topology without any pre-existing infrastructure. Combined with millimeter-wave (mmWave), Ad-hoc networks can construct communication links with less time and higher directivity due to directional antennas and building blockage. The wide spectrum of mmWave could provide a high-oriented channel for positioning, which is significant for multi-user conditions. In this paper, we concentrate on high-efficiency algorithms to allocate spectrum and power to different services and achieve a performance tradeoff between the communication and positioning process. Besides, the severe interference between users would degrade the actual system performance. To address these challenges, this paper proposes an optimal clustering algorithm based on the mmWave Line of Sight (LoS) probability to form two different sub-nets for communication and positioning services, respectively. Then, the available spectrum resources are divided into two parts for the above sub-nets under the Filtered-Orthogonal Frequency Division Multiplexing (F-OFDM) technique, which could design sub-bands independently. Finally, we proposed an optimal algorithm to allocate sub-bands and power to improve the performance of the communication sub-net while guaranteeing the positioning performance in the corresponding sub-net. Numeric simulation results demonstrate that the proposed resource allocation algorithm could achieve better performance both in the communication and position process.**

***Index Terms*—Joint communication and positioning, Millimeter-wave, Clustering algorithm, Resource allocation, Ad hoc network.**

I. Introduction

JOINT communication and positioning is expected to be a key technique in promoting the construction of connected and autonomous vehicles (CAVs) networks [1], smart cities [2], and the Internet of Things (IoT) [3]. With the ever-increasing demand for precise positioning in many emerging applications, the Global Navigation Satellite System (GNSS) with meter-level accuracy has become increasingly inadequate in providing high performance, seamless, wide-area location services [4], especially in indoor environments, valleys, and other harsh environments. An Ad hoc network is a system of wireless mobile nodes that can freely and dynamically self-organize an arbitrary and temporary network topology with less networking time consumption and no demand for pre-existing infrastructures [5]–[7]. As a convenient infrastructure-free communication tool, Ad hoc networks have also become an important positioning solution in harsh environments. Orthogonal Frequency Division Multiple Access (OFDMA) technology can divide the total system bandwidth into a set of orthogonal sub-carriers that can be allocated to multiple users for simultanous transmissions [8]. Each wireless mobile node in the OFDMA Ad hoc network can transmit signals directly with other nodes without the eNB. With the enormous available bandwidth, it is also attractive for Ad hoc networks to operate in the mmWave frequencies. In addition, mmWave Ad hoc systems may experience less interference due to directional antennas and building blockage [9]. As two key enablers for future wireless systems [10]–[14], the application of mmWave and massive multiple-input multiple-out (MIMO) technologies would confer higher multi-path resolution in both time and angular domains and could enable high-accuracy positioning [15]. Hence, combined with such technologies, it would be beneficial to deliver flexible and thorough joint communication and positioning services that could realize a high-oriented position and high-rate communication simultaneously based on mmWave Ad hoc networks [9], [16], especially for Base Station (BS)-free scenarios [17].

In joint systems, the communication performance can be improved at the cost of reducing the sensing performance [18], which is the performance trade-off between two services. To realize a trade-off between the communication and positioning services, there would always be a resource competition in joint communication and positioning. This emphasizes the importance of efficient resource allocation algorithms when the available resources are limited, such as time slot, frequency spectrum, and power. In [19], the author states the relationship between achievable position quality and data rate in different beam training times. Based on [19], the author redistributes the wireless transmission frame structure with the initial access part, data transmission part, and position part [20]. In addition, the optimal tradeoff between communication capability and positioning quality is posed based on different mmWave beam

This work was supported in part by the National Natural Science Foundation of China under Grant 62132004 and in part by the MOST Major Research and Development Project under Grant 2021YFB2900204. *(Corresponding Author: Xiaofeng Lu.)*

Manuscript received xxxx 00, 0000; revised xxxx 00, 0000.

Xueni Luo, Xiaofeng Lu and Benquan Yin are with the State Key Laboratory of Integrated Services Networks, Xidian University, Xian 710071, China.(email: lxn@stu.xidian.edu.cn; luxf@xidian.edu.cn; bqyin@stu.xidian.edu.cn)

Kun Yang is with the School of Computer Science and Electronic Engineering, University of Essex, Colchester, CO4 3SQ U.K. (email: kunyang@essex.ac.uk)

training strategies in [21], [22]. Nevertheless, they do not consider the specific resource allocation algorithm but only the beam training. In [23], [24], the authors propose an optimal power allocation scheme to minimize the average positioning error while satisfying the quality of services (QoS) demand and power budget constraints. They achieve the tradeoff between communication and positioning. However, they do not consider other effect elements to acquire more general conclusions. In [25], the author investigates different time-frequency resource allocation strategies in an mmWave framework considering communication and localization services in a multi-user multi-carrier case. However, their resource allocation algorithms regard the time-frequency block as the minimum unit in lack of the element of sub-carrier and could not fit the actual changing needs.

In addition to communication and positioning performance, joint communication and positioning also needs to guarantee the QoS demand for each user in a multi-user case. [26] investigates the channel width self-adaption scheme for OFDMA multi-hop Ad hoc networks, which leads to rewarding resource allocation. However, for quintessential Orthogonal Frequency Division Multiplexing (OFDM) or OFDMA, there would be only one default parameter setting mode in the air interface technology, such as fixed cyclic prefix, sub-carrier interval, etc, which makes them formidable to support diversified application scenarios [27], [28]. Therefore, [29] proposes the concept of F-OFDM, which is evolved from OFDM and extended to be a more applicable technology in virtue of lower spectrum leakage and smaller out-of-band interference by setting sub-band filters at the transmitting and receiving terminals. And [30] examines a multi-service resource allocation method in the F-OFDM system. However, the author does not mention joint communication and positioning. The growing number of users will cause more serious multi-user interference, which would significantly degrade communication and positioning performance. In [31], the author studies beam selection and power allocation problems, and achieves a large rate-accuracy region compared to conventional schemes. However, it ignores the interference between users. For this aspect, [32] made researches on cluster schemes based on mmWave LoS probability to enhance the connectivity among a single cluster against severe path loss from None Line of Sight (NLoS) scenarios. Combined with optimal resource allocation algorithms and effective clustering schemes, joint communication and positioning based on mmWave Ad hoc networks and F-OFDM could realize better comprehensive performance with little interference.

The quality of experience in wireless networks highly depends on both the accuracy of positioning awareness [33] and the communication capability. To the best of our knowledge, in the context of joint communication and positioning, there is no existing work about addressing the demand for flexible division of frequency spectrum and power which could achieve positioning awareness and communication capability for the mmWave Ad hoc system based on F-OFDM. Against the existing approaches, the key contributions of this paper are as follows:

- Considering to adapt to the different characteristics of communication and positioning service, we establish a joint communication and positioning system model based on F-OFDM in mmWave multi-hop Ad-hoc networks. According to the different service functions, we reconstruct the integrated network into an independent communication network and positioning network.
- We use the LoS probability between users to be the similarity metric for clustering, and propose the modified LoS-AP clustering algorithm for mmWave systems to form two independent sub-nets for different demands of communication and positioning services. And each sub-net would be transferred into several non-intersecting and non-overlapping clusters.
- We divide the feasible spectrum into two sub-nets based on F-OFDM and investigate the joint resource allocation problem in two sub-nets corresponding to sub-bands and power. We could solve it with a modified Generalized Benders Decomposition (GBD) algorithm, in which the basic idea is to decompose the primal problem into two iterative sub-problem. The proposed effective allocation scheme could achieve a higher sum rate in the constraint of positioning accuracy.

The rest of this paper is organized as follows: Section II describes the mmWave channel property and comprehensive system model. Section III introduces the performance metrics and cluster methods. Section IV presents the optimization problem and proposed transmission scheme. Section V shows the simulation results. Finally, the conclusions are stated in Section VI.

Notations: The transpose, conjugate, and conjugate transpose are denoted by $(\cdot)^{\mathrm{T}}$, $(\cdot)^{*}$, and $(\cdot)^{\mathrm{H}}$, respectively. $\mathrm{E}\{\cdot\}$ denotes the expectation of any estimation variables.

II. System model

This section describes the mmWave channel model for communication and positioning respectively, and the joint communication and positioning system model in the mmWave Ad hoc network based on F-OFDM. The mathematical representations for mmWave received signal are also presented here, which are prepared for defining performance metrics and the proposed transmission scheme in the next section.

A. MmWave channel model

Accounting for the unfavorable drawbacks of NLoS scenarios, the subsection would only consider LoS paths [34], [35].

1) Path loss model: In 3GPP, there are massive well-known channel models broadly employed in industry, such as UMi, UMa, etc [36]. They provide key channel parameters including LoS probabilities, path loss models, path delays, and path power levels. The Free Space Path Loss (FSPL) model usually be used to describe the loss of LoS paths over distance at all relevant frequencies [35]. As a standardized basic modeling method, the FSPL model determine the path loss with distance and frequency and can be written as:

$$\mathrm{FSPL}\left(f_c, d_{i,j}\right) = 32.4 + 20\log_{10}\left(d_{i,j}\right) + 20\log_{10}\left(f_c\right), \tag{1}$$

where d_{ij} and f_c are the Euclidean distance between node *i* and *j* in 2-Dimension and the carrier frequency, respectively. From (1), $d_{i,j}$ could be expressed as:

$$d_{ij} = 10^{\frac{\text{Loss}_{ij} - 20\log_{10}(f_c) - 32.4}{20}}, \tag{2}$$

where Loss_{ij} is the mmWave path loss between node *i* and *j*.

According to the standard of 3GPP TR 38.901 for UMi scenarios, mmWave LoS probability between node *i* and node *j* could be presented by

$$\begin{aligned} P_{i,j}^{LOS} = &\min\left(\frac{d_1}{d_{ij}}, 1\right)\left(1 - \exp\left(\frac{-d_{ij}}{d_2}\right)\right) \\ &+ \exp\left(\frac{-d_{ij}}{d_2}\right), \end{aligned} \tag{3}$$

where $P_{i,j}^{LOS}$ is the mmWave LoS probability, namely it could distinguish LoS path to some extent, d_1 and d_2 are fit parameters with constant values.

2) Positioning model: In the mmWave MIMO systems, it is possible to estimate distances and angles accurately by a large bandwidth and beamforming [37], [38]. Consider a wireless mmWave downlink scenario consisting of a known anchor node equipped with N_t antenna elements and two user nodes, each equipped with N_r antenna elements. The precoding vector of the anchor node for *n*-th sub-carrier is denoted as $\boldsymbol{f}_n \in \mathbb{C}^{N_t}$. Thus, these two user nodes' positions relative to the anchor node are illustrated in Fig.1, given as $\boldsymbol{p}_u = [p_x^u, p_y^u]^{\mathrm{T}} \in \mathbb{R}^2$. Fig.1 also describes the LoS mmWave channel parameters including $\phi_u \in [0, \pi)$, $\theta_u \in [0, \pi)$, and τ_u, which are angles of arrival (AoA), angles of departure (AoD), and time delay respectively.

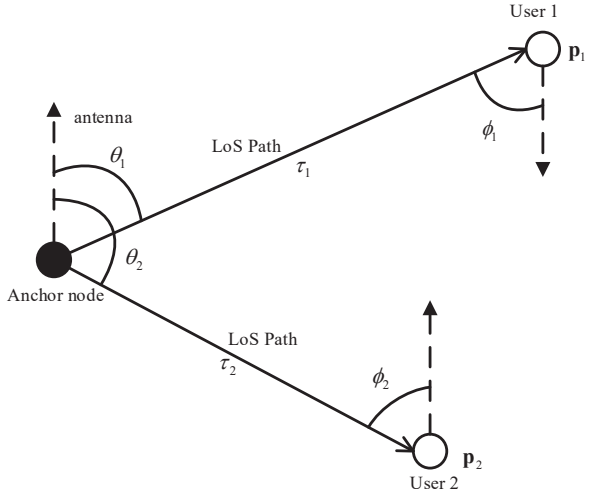

Fig. 1. Example of deployment with 1 anchor node and two user nodes at location $\boldsymbol{p}_1$ and $\boldsymbol{p}_2$ respectively.

In fact, there are multi-path components (MPCs) in the mmWave communication. However, when no prior knowledge of range biases is available, NLoS signals make no contribution to the Equivalent Fisher's Information Matrix (EFIM) for the positioning [39]. So the positioning model only needs to consider the LoS path.

Assume that the complex signal is transmitted across *N* continuous sub-carriers centered around frequency f_c with bandwidth *B*. Then the $N_r \times N_t$ complex positioning channel matrix for *n*-th sub-carrier between anchor node and *u*-th user node is denoted by $\boldsymbol{H}_{p,u}^n$ and is formulated as in [40]:

$$\boldsymbol{H}_{p,u}^n = \sqrt{\text{Loss}_{p,u}} h_{p,u} e^{-j2\pi\tau_{p,u}\frac{nB}{N}} \boldsymbol{a}_{R,u}\left(\phi_{p,u}\right) \boldsymbol{a}_{T,u}^{\mathrm{H}}\left(\theta_{p,u}\right), \tag{4}$$

where $\text{Loss}_{p,u}$ denotes the average path loss between anchor node and *u*-th user node, and $h_{p,u} \in \mathbb{C}$ is the channel coefficient. Consider two uniform linear arrays (ULA) for transmitting antenna and receiving antenna with an odd number of antenna elements. And the transmitting antenna array response could be presented by

$$\boldsymbol{a}_{T,u}(\theta_{p,u}) = \frac{1}{\sqrt{N_t}}\left[e^{-j\left(\frac{N_t+1}{2}-1\right)Z}, \ldots, e^{-j\left(\frac{N_t+1}{2}-N_t\right)Z}\right]^T, \tag{5}$$

with $Z = \frac{2\pi}{\lambda_c} d\cos\left(\theta_{p,u}\right)$.

In (5), λ_c denotes the wavelength corresponding to the center frequency of transmitted signals, and *d* is the inter-element distance. Similarly, $\boldsymbol{a}_{R,u}\left(\phi_{p,u}\right)$ could be derived by exchanging $\theta_{p,u}$, N_t with $\phi_{p,u}$ and N_r in (5) respectively.

3) Communication model: Assumed that there are *L* MPCs in the mmWave communication between user node *u* and *i*, the $N_r \times N_t$ complex communication channel matrix for *n*-th sub-carrier between user node *u* and *i* is denoted by $\boldsymbol{H}_{c,iu}^n$ and is formulated as:

$$\begin{aligned} &\boldsymbol{H}_{c,iu}^n = \\ &\sqrt{\text{Loss}_{c,iu}} \sum_{l=1}^{L} h_{c,iu}^l e^{-j2\pi\tau_{c,iu}^l \frac{nB}{N}} \boldsymbol{a}_{R,iu}\left(\phi_{c,iu}^l\right) \boldsymbol{a}_{T,iu}^{\mathrm{H}}\left(\theta_{c,iu}^l\right). \end{aligned} \tag{6}$$

in which the parameters are similar to that in the positioning channel model. Therefore, for user node *u*'s transmitted signal denoted by $s_{n,u}$, the corresponding user node *i*'s received signal $\boldsymbol{y}_{iu}^n$ could be expressed as:

$$\boldsymbol{y}_{iu}^n = \sqrt{P_u}\boldsymbol{w}_i^{\mathrm{H}} \boldsymbol{H}_{c,iu}^n \boldsymbol{f}_n s_{n,u} + \tilde{\mathbf{n}}, \tag{7}$$

where P_u is the transmitted power with respect to the *u*-th user node. $\boldsymbol{w}_i \in \mathbb{C}^{N_r}$ denotes the beamforming vector in the *i*-th user node. $\tilde{\mathbf{n}}$ is the additional white Gaussian noise (AWGN) with zero mean and $N_0/2$ variance.

B. Joint communication and positioning system model

The comprehensive system model in mmWave Ad hoc system with F-OFDM is illustrated as Fig.2. In Fig.2(a), there exist 18 unknown user nodes and 3 known anchor nodes, among which user nodes would experience communication and positioning services in the initial topological network. When each node communicates with each other through F-OFDM signal, the target nodes can also be located by receiving F-OFDM signal from the anchor node, and the sub-bands used for positioning service are different from that for communication service. Besides, the anchor nodes are only regarded as indispensable for positioning the user nodes, as declared in Section II-A.

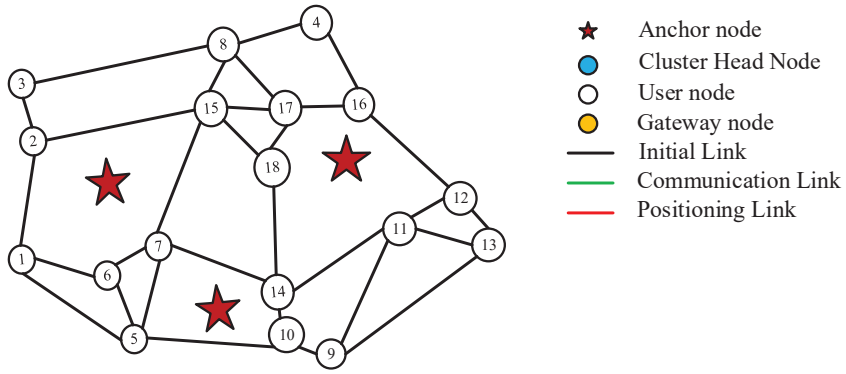

(a) Initial topological network with 3 anchor nodes and 18 user nodes.

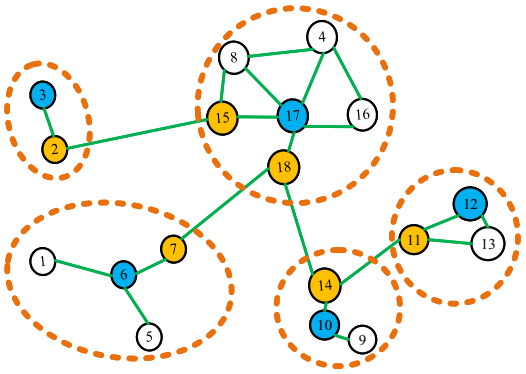

(b) Communication sub-nets with 5 clusters.

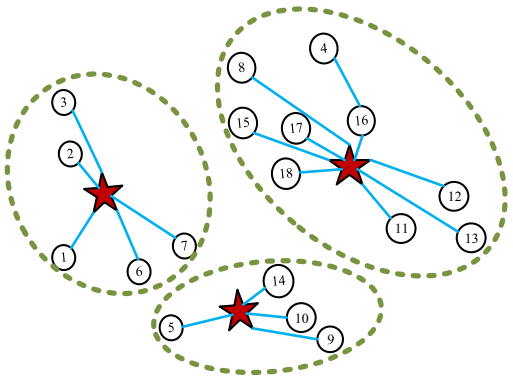

(c) Position sub-nets with 3 clusters around anchor nodes.

Fig. 2. Joint communication and positioning system model and communication and position sub-nets.

When the network only provides communication services, Fig.2(a) can be simplified to Fig.2(b), all user nodes have the same identity to send/receive communication signals. When the network only provides the positioning service, Fig.2(a) can be simplified to Fig.2(c), the nodes in the network are distinguished as the anchor nodes and the target nodes which need to be located. The target node receives the signal from the anchor node and obtains its own location information through the positioning algorithm and calculating the receiving signal waveform parameters which are not the focuses of this paper. In other words, the initial topological network is divided into two sub-nets, the communication sub-net and the positioning sub-net. Each sub-net includes several clusters. As for Fig.2(b), all user nodes are clustering into 5 clusters on account of the communication services. In each cluster in Fig.2(b), the blue user nodes denote the cluster head node to transmit information and control resource allocation in its cluster and the yellow user nodes denote the gateway node to forward information between different clusters. According to Fig.2(c), the user nodes would be clustered around each most suitable anchor node for the positioning services by the proposed clustering algorithm which would be introduced in Section IV in detail. And the anchor nodes play the role of controlling resource allocation for positioning.

In [41], the author deduced the target node's position from the received signal sent by the anchor node, and show that the positioning accuracy is determined by the network topology, channel condition, signal waveform and transmission power. In the resource-limited wireless positioning network, the network topology and channel conditions are usually determined by the external environment, so the reasonable resource allocation to nodes including power, bandwidth and carrier frequency is the key tool to improve positioning accuracy. In our network, the sub-carriers and power should be mainly allocated to user nodes and anchor nodes to process the communication and position services. Assume that there are N sub-carriers, and the transmit power is presented by P_{total}. Owing to F-OFDM, all sub-carriers could be composed into different orthogonal resource blocks (RB) by sliding windows of variable length. Subsequently, RBs would randomly constitute different sub-bands, avoiding overlapping between the communication and positioning spectrum to reduce the co-channel interference. In Fig.3, after clustering, the user nodes in the same cluster use the orthogonal sub-bands to reduce the interference between user nodes. In general, the same sub-bands could be implemented in two or more clusters if and only if the two or more point-to-point links in different clusters do not contain a common node in the multi-hop communication process, while the same sub-bands could be implemented in two or more positioning clusters since positioning clusters are independent and devoid of any links, which saves the resources in the same conditions.

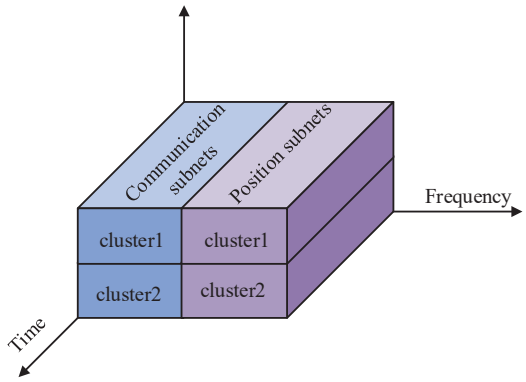

Fig. 3. Frequency division multiplexing model in communication and position sub-nets.

Finally, their sub-nets would have different sub-bands and power allocation schemes to process communication and positioning services to improve comprehensive performance.

III. Performance metrics

A. Positioning accuracy

For an unknown user node, it is crucial to measure its parameters and link with an adjacent anchor node, comprising AoA, AoD, time delay, Cartesian coordinates, relative direction angle α_u, and channel coefficient. However, an angle measurement is difficult and expensive, much less than the estimation process. Hence, consider $\boldsymbol{\mu}_u = \left[p_x^u, p_y^u, \alpha_u, H_u^R, H_u^I\right]$ be the vector including the estimation variables of *u*-th user node to characterise the position error bounds. H_u^R, H_u^I are the real and imaginary channel coefficients, respectively.

It is known that the mean squared error matrix of any unbiased single parameter for deterministic parameters and any other estimators of the random parameter is bounded by Cramér–Rao Lower Bound (CRLB), which equals the inverse of Fisher information matrix (FIM) as

$$\mathrm{E}\left\{\left(\widehat{\boldsymbol{\mu}}_u - \boldsymbol{\mu}_u\right)\left(\widehat{\boldsymbol{\mu}}_u - \boldsymbol{\mu}_u\right)^{\mathrm{T}}\right\} \succcurlyeq \boldsymbol{J}_u^{-1}, \tag{8}$$

where $\widehat{\boldsymbol{\mu}}_u$ is the unbiased estimator of $\boldsymbol{\mu}_u$, and $\boldsymbol{J}_u \in \mathbb{R}^{5\times 5}$ denotes the FIM for $\boldsymbol{\mu}_u$, computed by

$$\boldsymbol{J}_u \triangleq \boldsymbol{E}_{\mathbf{y}|\boldsymbol{\mu}_u}\left[-\frac{\partial^2 \ln f\left(\mathbf{y} \mid \boldsymbol{\mu}_u\right)}{\partial \boldsymbol{\mu}_u \partial \boldsymbol{\mu}_u^{\mathrm{T}}}\right], \tag{9}$$

where $f\left(\mathbf{y}|\boldsymbol{\mu}_u\right)$ is the likelihood function of the random received vector $\mathbf{y}$ with $\boldsymbol{\mu}_u$ as a condition and expressed as:

$$f\left(\mathbf{y}|\boldsymbol{\mu}_u\right) \propto \exp\left\{\frac{1}{N_0}\sum_{n=-N/2}^{N/2}\left(2\Re\left(\boldsymbol{\zeta}_n^{\mathrm{H}}\mathbf{y}^n\right) - \|\boldsymbol{\zeta}_n\|_2^2\right)\right\}, \tag{10}$$

where $\boldsymbol{\zeta}_n \triangleq \mathbf{H}_{p,u}^n \boldsymbol{w}_r \boldsymbol{f}_n$, $\propto$ represents an equivalence relation independent of constants.

The utilization of CRLB as a performance metric for positioning is desirable due to its tractability and its asymptotical achievability in high SNR regimes [37], and the corresponding FIM for (8) would be computed by (9) and (11), where the values of the matrix entries are given in Appendix A.

$$\boldsymbol{J}_u = \sum_{n=-N/2}^{N/2} \boldsymbol{J}_{u,n}, \tag{11}$$

where $\boldsymbol{J}_{u,n}$ is FIM of the *n*-th sub-carrier and is presented as shown at the bottom of this page with the order of (12) [40].

In addition, we only consider the dominant LoS paths in calculating (9) and (11) to reduce the complexity of inverting the matrix for the derivation of CRLB. Although the MPCs independently contribute to the FIM as N_r and B increases theoretically, it is demonstrated in [41], [42] that the CRLB on the position is negatively affected only by the first-contiguous MPCs if LoS paths are present together with MPCs, which affirmed the feasibility of this computed strategies.

Hence, there are two relative concepts for characterizing *u*-th user node's positioning accuracy, Position Error Bound (PEB) and Orientation Error Bound (OEB), which could be expressed by [40]:

$$\mathrm{PEB}_u = \sqrt{\mathrm{trace}\left(\boldsymbol{J}_{u,1:2,1:2}^{-1}\left(\boldsymbol{X}_N\right)\right)}, \tag{13}$$

$$\mathrm{OEB}_u = \sqrt{\boldsymbol{J}_{u,3,3}^{-1}\left(\boldsymbol{X}_N\right)}, \tag{14}$$

where $\boldsymbol{X}_N \in \mathbb{C}^{M\times M}$ is defined as the block diagonal matrix consisting of the matrix $\boldsymbol{F}_n$ over each sub-carrier with $M = N_t \times N$ and $\boldsymbol{F}_n = \boldsymbol{f}_n \boldsymbol{f}_n^H$, expressed as

$$\boldsymbol{X}_N = \begin{bmatrix} \boldsymbol{F}_1 & & & \\ & \boldsymbol{F}_2 & & \\ & & \ddots & \\ & & & \boldsymbol{F}_N \end{bmatrix}. \tag{15}$$

B. Data rate

Within a channel coherence time T_c, we assume that a user only transmits signals to another user, i.e. point-to-point communication. Based on Shannon Theory, all feasible LoS paths have their optimal sub-bands bandwidth and transmitted power owing to inequable channel gain, in the mmWave Ad hoc network based on F-OFDM.

From the received signal in (7), the *i*-th user node received signal-noise ratio (SNR) based on the signal transmitted by the *u*-th user node could be presented as [31]:

$$\begin{aligned}
\mathrm{SNR}_u &= \frac{1}{N_0}\sum_{n=n_1}^{n_N} P_u \left|\boldsymbol{w}_i^{\mathrm{H}} \boldsymbol{H}_{c,iu}^n \boldsymbol{f}_n\right|^2 |s_{n,u}|^2 \\
&= \frac{1}{N_0}\sum_{n=n_1}^{n_N} P_u |s_{n,u}|^2 \,\mathrm{Loss}_{c,iu} |h_{c,iu}|^2 \left|\boldsymbol{w}_i^{\mathrm{H}} \boldsymbol{a}_{R,iu}\right|^2 \boldsymbol{a}_{T,iu}^H \boldsymbol{F}_n \boldsymbol{a}_{T,iu} \\
&= \frac{1}{N_0} \boldsymbol{a}_{\zeta,iu}^{\mathrm{H}} \boldsymbol{X}_N \boldsymbol{a}_{\zeta,iu} \\
&= \frac{1}{N_0} P_u^{\boldsymbol{C}},
\end{aligned} \tag{16}$$

with

$$\boldsymbol{a}_{\zeta,iu}^{\mathrm{H}} = \left[\begin{array}{cccc} \zeta_u |s_{n_1,u}| \boldsymbol{a}_{T,iu}^{\mathrm{T}} & \cdots & \zeta_u |s_{n_N,iu}| \boldsymbol{a}_{T,iu}^{\mathrm{T}} \end{array}\right]^{\mathrm{T}}, \tag{17}$$

where $\zeta_u = \sqrt{P_u \operatorname{Loss}_{c,iu}}\,|h_{c,iu}|\left|\boldsymbol{w}_i^{\mathrm{H}}\boldsymbol{a}_{R,iu}\right|$.

The data rate for the u-th user node could be formulated as

$$R_u = B_u^{\boldsymbol{C}} \log_2\left(1+\mathrm{SNR}_u\right), \tag{18}$$

where $B_u^{\boldsymbol{C}}$ denotes the allocated transmitted sub-bands corresponding to $P_u^{\boldsymbol{C}}$ in the communication process.

Hence, the sum rate for U users, can now be expressed by

$$\begin{aligned} R = \sum_{u=1}^{U} R_u &= \sum_{u=1}^{U} B_u^{\boldsymbol{C}} \log_2\left(1+\mathrm{SNR}_u\right) \\ &= \sum_{u=1}^{U} B_u^{\boldsymbol{C}} \log_2\left(1+\frac{P_u^{\boldsymbol{C}}}{N_0}\right). \end{aligned} \tag{19}$$

In reality, the estimated channel state information (CSI) is imperfect. In this case, the anchor node treats the estimated channels as the true channels which could be indicated by the design of $\boldsymbol{f}_n$ and $\boldsymbol{w}_i$. Then N_0 in (19) is assumed by treating the interuser interference and the interference from the channel estimation error as a part of the effective noise in (16) [31].

IV. Proposed transmission scheme

This section presents an optimization problem for designing sub-bands and power allocation schemes. Most joint communication and positioning scenarios must guarantee required position accuracy while generating a high data rate for user nodes. In this regard, the resource allocation problem considering position accuracy and communication capability is formulated first, and then the corresponding transmission schemes are derived.

A. Problem formulation

Consider a mmWave Ad hoc network with F-OFDM consisting of U user nodes and K anchor nodes. Each node is equipped with an F-OFDM radio. The transmission range of each node is set to be d^*. And the problem formulation here adopts the optimal beamformers design both for anchor nodes and user nodes whatever the sub-bands are allocated in [19]. This could be expressed as a joint optimization problem with two control variables, which could be presented by

$$\mathcal{S}^{\boldsymbol{P}} \triangleq \left\{\mathrm{PEB}_u, \mathrm{OEB}_u, P_u^{\boldsymbol{P}}, B_u^{\boldsymbol{P}}\right\}_{u=1}^{U}, \tag{20a}$$

$$\mathcal{S}^{\boldsymbol{C}} \triangleq \left\{R_u, P_u^{\boldsymbol{C}}, B_u^{\boldsymbol{C}}\right\}_{u=1}^{U}, \tag{20b}$$

$$\mathcal{S}^{\boldsymbol{G}} \triangleq \left\{\mathcal{S}^{\boldsymbol{P}}, \mathcal{S}^{\boldsymbol{C}}\right\}_{u=1}^{U}, \tag{20c}$$

where $P_u^{\boldsymbol{P}}$ and $B_u^{\boldsymbol{P}}$ are denoted the allocated transmitted power and sub-bands like $P_u^{\boldsymbol{C}}$ and $B_u^{\boldsymbol{C}}$, but for the positioning process.

Utilizing (20), the feasible sets for the optimization problem are expressed to consider the constraints as

$$\begin{aligned} \check{\mathcal{S}}^{\boldsymbol{P}} \triangleq \big\{\mathcal{S}^{\boldsymbol{P}}:\ & \mathrm{PEB}_u \le \varepsilon_u^{\mathrm{PEB}}, \forall u && \text{(21a)}\\ & \mathrm{OEB}_u \le \varepsilon_u^{\mathrm{OEB}}, \forall u && \text{(21b)}\\ & \sum_{u=1}^{U} P_u^{\boldsymbol{P}} \le P_{total}^{\boldsymbol{P}} && \text{(21c)}\\ & \sum_{u=1}^{U} B_u^{\boldsymbol{P}} \le B_{total}^{\boldsymbol{P}} && \text{(21d)}\\ & P_u^{\boldsymbol{P}} \succeq 0, \forall u, && \text{(21e)}\\ & B_u^{\boldsymbol{P}} \succeq 0, \forall u.\ \big\} && \text{(21f)} \end{aligned}$$

$$\begin{aligned} \check{\mathcal{S}}^{\boldsymbol{C}} \triangleq \big\{\mathcal{S}^{\boldsymbol{C}}:\ & R_u \ge R_u^*, \forall u && \text{(22a)}\\ & \sum_{u=1}^{U} P_u^{\boldsymbol{C}} \le P_{total}^{\boldsymbol{C}}, && \text{(22b)}\\ & \sum_{u=1}^{U} B_u^{\boldsymbol{C}} \le B_{total}^{\boldsymbol{C}}, && \text{(22c)}\\ & P_u^{\boldsymbol{C}} \succeq 0, \forall u && \text{(22d)}\\ & B_u^{\boldsymbol{C}} \succeq 0, \forall u\ \big\} && \text{(22e)} \end{aligned}$$

$$\begin{aligned} \check{\mathcal{S}}^{\boldsymbol{G}} \triangleq \big\{\mathcal{S}^{\boldsymbol{G}}:\ & P_{total}^{\boldsymbol{P}} + P_{total}^{\boldsymbol{C}} \le P_{total} && \text{(23a)}\\ & B_{total}^{\boldsymbol{P}} + B_{total}^{\boldsymbol{C}} \le B_{total}\ \big\} && \text{(23b)} \end{aligned}$$

The constraints in (21a) and (21b) are the requirements of the PEB and OEB where the right values denote the highest position error bound for all user nodes. Similarly, the constraint in (22a) is the lowest data rate for all user nodes. The power constraints are satisfied with (21c), (21e), (22b), (22d), and (23a). And the remaining are constraints about sub-bands allocation.

From (19), (20), (21), (22), and (23), the optimization problem is formulated as

$$\begin{aligned} \mathscr{P}_1 : \underset{\mathcal{S}^{\boldsymbol{P}},\mathcal{S}^{\boldsymbol{C}},\mathcal{S}^{\boldsymbol{G}}}{\text{maximize}} & \sum_{u=1}^{U} B_u^{\boldsymbol{C}} \log_2\left(1+\mathrm{SNR}_u(P_u^{\boldsymbol{C}})\right) && \text{(24)}\\ \text{subject to}: \ & \mathcal{S}^{\boldsymbol{P}} \subseteq \check{\mathcal{S}}^{\boldsymbol{P}}, \\ & \mathcal{S}^{\boldsymbol{C}} \subseteq \check{\mathcal{S}}^{\boldsymbol{C}}, \\ & \mathcal{S}^{\boldsymbol{G}} \subseteq \check{\mathcal{S}}^{\boldsymbol{G}}. \end{aligned}$$

Since the sub-bands could not be multiplexed by communications and positioning for a single user node, $\mathscr{P}_1$ could be decomposed into two sub-problems. The first sub-problem is for the positioning process, in which the requirements for accuracy are satisfied with the minimum power and (nearly) optimal sub-bands, expressed by

$$\mathscr{P}_2 : \underset{\mathcal{S}^{\boldsymbol{P}}}{\text{minimize}} \quad P_{total}^{\boldsymbol{P}} + \boldsymbol{\gamma} B_{total}^{\boldsymbol{P}} \tag{25}$$

$$\boldsymbol{J}_{u,n} = \begin{bmatrix} \Phi_n\left(p_x^u, p_x^u\right) & \Phi_n\left(p_x^u, p_y^u\right) & \Phi_n\left(p_x^u, \alpha_u\right) & \Phi_n\left(p_x^u, H_u^R\right) & \Phi_n\left(p_x^u, H_u^I\right) \\ \Phi_n\left(p_y^u, p_x^u\right) & \Phi_n\left(p_y^u, p_y^u\right) & \Phi_n\left(p_y^u, \alpha_u\right) & \Phi_n\left(p_y^u, H_u^R\right) & \Phi_n\left(p_y^u, H_u^I\right) \\ \Phi_n\left(\alpha_u, p_x^u\right) & \Phi_n\left(\alpha_u, p_y^u\right) & \Phi_n\left(\alpha_u, \alpha_u\right) & \Phi_n\left(\alpha_u, H_u^R\right) & \Phi_n\left(\alpha_u, H_u^I\right) \\ \Phi_n\left(H_u^R, p_x^u\right) & \Phi_n\left(H_u^R, p_y^u\right) & \Phi_n\left(H_u^R, \alpha_u\right) & \Phi_n\left(H_u^R, H_u^R\right) & \Phi_n\left(H_u^R, H_u^I\right) \\ \Phi_n\left(H_u^I, p_x^u\right) & \Phi_n\left(H_u^I, p_y^u\right) & \Phi_n\left(H_u^I, \alpha_u\right) & \Phi_n\left(H_u^I, H_u^R\right) & \Phi_n\left(H_u^I, H_u^I\right) \end{bmatrix}, \tag{12}$$

$$\text{subject to}: \mathcal{S}^{\boldsymbol{P}} \subseteq \check{\mathcal{S}}^{\boldsymbol{P}}.$$

After solving Problem $\mathscr{P}_2$, the remaining power and sub-bands set for the communication process could be determined owing to (23a) and (23b). Then the second sub-problem's objective is to maximize the data rate, as follows

$$\begin{aligned} \mathscr{P}_3: \underset{\mathcal{S}^{\boldsymbol{C}},\mathcal{S}^{\boldsymbol{G}}}{\text{maximize}} & \sum_{u=1}^{U} B_u^{\boldsymbol{C}} \log_2\left(1+\mathrm{SNR}_u(P_u^{\boldsymbol{C}})\right) \\ \text{subject to}: & \mathcal{S}^{\boldsymbol{C}} \subseteq \check{\mathcal{S}}^{\boldsymbol{C}}, \\ & \mathcal{S}^{\boldsymbol{G}} \subseteq \check{\mathcal{S}}^{\boldsymbol{G}}. \end{aligned} \tag{26}$$

According to Problem $\mathscr{P}_2$, and $\mathscr{P}_3$, the next subsections propose an optimal transmission scheme.

B. Clustering scheme

In the mmWave Ad hoc network, it is crucial to allocate resources to nodes whose links are LoS to maximize data rate. Hence, this subsection proposed a clustering scheme based on LoS probability. The anchor nodes operate as the CHs as Section II-B depicted for the positioning process, and the accuracies should be coordinated. In addition, it is illogical to perform intra-cluster positioning process, which means the clustering scheme has little effect on the positioning process. And for the communication process, it is indispensable to design a cluster scheme to program the resource allocation in communication links when allowed for resource multiplexing.

The clustering scheme is developed by the LoS probability, and the objective is to maximize the LoS probabilities in the topology, which is similar to the basic idea of the Affinity Propagation algorithm (AP) [43]. AP algorithm inputs the concrete similarity matrix, $s(i,k) \in \mathbb{R}^{U\times U}$, which U equals the overall number of users. The diagonal elements are defined as $p(i)$ and output the unique clustering result. Moreover, AP would lead into two essential matrixes, namely responsibility matrix $r(i,j)$, and availability matrix $a(i,j)$, as follows

$$r_{t+1}(i,k) = \begin{cases} s(i,k) - \max\limits_{j\neq k}\left\{a_t(i,j)+s(i,j)\right\}, & i \neq k \\ p(k) - \max\left(a_{t+1}(i,j), s(i,j)\right), & i = k \end{cases} \tag{27}$$

where the responsibility matrix elements are set zero before iterations and denote how well-suited node *k* is to serve as the CH of node *i*, taking into account other nodes for node *i*.

$$a_{t+1}(i,j) = \begin{cases} \min\limits_{i\neq k}\left\{0, r_t(j,j) + \sum\limits_{j\neq i,k}\left\{\max\left(0, r_t(j,k)\right)\right\}\right\}, \\ \sum \max\limits_{j\neq k, i=k}\left(0, r_t(j,k)\right), \end{cases} \tag{28}$$

where the availability matrix elements denote how well-suited node *i* regard node *k* as the CH and are initialized to be zero.

And the iteration processes of responsibility matrix and availability matrix could be formulated as

$$r_{t+1}(i,k) = (1-\beta)r_{t+1}(i,k) + \beta r_t(i,k), \tag{29a}$$

$$a_{t+1}(i,k) = (1-\beta)a_{t+1}(i,k) + \beta a_t(i,k), \tag{29b}$$

where $\beta \in (0,1)$ represents a damping factor to promote convergence. β is introduced to attenuate the attraction and attribution information. In the iteration process, the responsibility and availability matrix of the previous generation will have an impact on that of the current generation, and the weight of the influence is adjusted by β. When the number of clusters generated by our modified Los-AP algorithm keeps changing during the iteration process, and the algorithm can not converge, increasing β can eliminate the oscillation and improve the convergence rate.

Hence, we modify the input as the LoS probability between nodes computed by (3) to maximize the LoS probability and to allocate resources effectively, which the diagonal elements are formulated as

$$p(i) = \lambda \cdot \text{average}\left\{s(i,k)\right\} \tag{30}$$

where λ is an impact factor for clustering radius to some extent. And the constraints on clustering are the maximum radius of final clusters which is less than or equal to the transmission range of nodes, expressed by $r_{max} \leq d^*$, where d^* is computed by (3) with a certain LoS probability η.

The inter-cluster communication challenge could be settled in this way. However, it is still unfeasible for communication links between two different clusters, namely multi-hop communication across clusters. The gateway nodes are chosen to treat as relay nodes then.

For the above scenario, it is conceivable that the possibility of realizing multi-hop communications is related to the clustering scheme because of the premise of the transmission range d^*. On account of it, clusters are considered as neighbors when existing $d_{i,j} \leq d^*$ and node *i*, node *j* are from different clusters. And the gateway nodes are the nodes that have the minimum value of $d_{i,j}$, which numbers are no less than 1 in each cluster. Likewise, the cluster would be considered a Sole Cluster with no neighbors.

Assume *G* clusters after clustering comprising of *U* user nodes. And the proposed clustering scheme for maximizing the LoS probabilities through all user nodes is summarized in Algorithm 1 and Algorithm 2.

C. Problem solved scheme

1) Positioning process: Since Problem $\mathscr{P}_2$ is a mixed-integer problem with non-convex constraints, which is difficult to be directly solved. Instead, we simplify Problem $\mathscr{P}_2$ by fixing the totally allocated sub-bands and power for positioning. In addition, the positioning accuracy constraints are satisfied for each user node, which can simplify this problem further.

Then $\mathscr{P}_2$ is transformed to

$$\mathscr{P}_{2,a}^{u}: \underset{\mathcal{S}_a^{\boldsymbol{P}}}{\text{minimize}} \quad B_{total}^{\boldsymbol{P}} \tag{31a}$$

$$\text{subject to}: \ \mathcal{S}_a^{\boldsymbol{P}} \subseteq \check{\mathcal{S}}_a^{\boldsymbol{P}}, \tag{31b}$$

$$P_u^{\boldsymbol{P}} = P_{total}^{\boldsymbol{P}} / U, \tag{31c}$$

where $\mathcal{S}_a^{\boldsymbol{P}} \triangleq \left\{\mathrm{PEB}_u, \mathrm{OEB}_u, B_u^{\boldsymbol{P}}\right\}_{u=1}^{U}$, and the constraints set $\check{\mathcal{S}}_a^{\boldsymbol{P}}$ could be expressed similarly by $\check{\mathcal{S}}_a^{\boldsymbol{P}} \triangleq \left\{\mathcal{S}_a^{\boldsymbol{P}} : (21a), (21b)\right\}$. (31c) is the power constraint by equally

Algorithm 1 Modified LoS-AP algorithm

Require : $s(i,k)$, for $i,k = 1,2,...,U$ and d^*
Initialization : $s(i,k) \leftarrow (3)$ when $i \neq k$,
$p(i) \leftarrow (30)$ when $i = k$,
$r_{max} = \infty$,

```
Set η, and d* ← (3),
while r_max > d* within max iterations do
    Itertion index: t = 1
    Node index: u = v = 0
    Matrix reset: r_t = a_t = 0
    repeat
        u ⇐ u + 1
        r_t(i,k) ← (27), (29a),
        a_t(i,k) ← (28), (29b),
    until u = U
    repeat
        v ⇐ v + 1
        Solve max_k {r_t(i,k) + a_t(i,k)}
        if k = i then set node i as CH,
        else set node k as CH of node i,
        end if
    until v = U
    if CH seletion changes then restart from 2;
    else t ⇐ t + 1
        Update r_max
        if r_max ≤ d* then break,
        else adjust p(i) by factor λ,
        end if
    end if
end while
return clustering results and η.
```

Algorithm 2 Gateway node seletion algorithm based on η

Require : clustering results and η,

```
while Sole Cluster exists within max iterations do
    adjust p(i) and turn to Algorithm 1
end while
if Sole Cluster does not exist then return,
else adjust η and turn to Algorithm 1
end if
return the optimal clustering results and gateway nodes selection.
```

distributed and $P_{total}^{\boldsymbol{P}}$ would be adjusted by the solution of $\mathcal{S}_b^{\boldsymbol{P}}$, which could be formulated as:

$$\mathscr{P}_{2,b}^{u}: \underset{\mathcal{S}_b^{\boldsymbol{P}}}{\text{minimize}} \quad P_{total'}^{\boldsymbol{P}} \tag{32a}$$

$$\text{subject to}: \ \mathcal{S}_b^{\boldsymbol{P}} \subseteq \check{\mathcal{S}}_b^{\boldsymbol{P}}, \tag{32b}$$

$$B_{total}^{\boldsymbol{P}}, \tag{32c}$$

where $\mathcal{S}_b^{\boldsymbol{P}} \triangleq \left\{\mathrm{PEB}_u, \mathrm{OEB}_u, P_u^{\boldsymbol{P}}\right\}_{u=1}^{U}$, and the constraints set $\check{\mathcal{S}}_b^{\boldsymbol{P}}$ could be expressed practically by $\check{\mathcal{S}}_b^{\boldsymbol{P}} \triangleq \check{\mathcal{S}}_a^{\boldsymbol{P}}$. (32c) is the sub-bands constraint which comes from Problem $\mathcal{S}_a^{\boldsymbol{P}}$.

Since $\mathcal{S}_a^{\boldsymbol{P}}$ is a prototypical resource allocation problem that could be solved by the Greedy Algorithm according to channel gain, we could get optimal sub-bands allocation concerning corresponding power when considering the resource multiplexing in different clusters. Then for Problem $\mathcal{S}_b^{\boldsymbol{P}}$, the objective function is to minimize the power for the positioning process in the constraint of sub-bands allocation given as Problem $\mathcal{S}_a^{\boldsymbol{P}}$. After solving Problem $\mathcal{S}_b^{\boldsymbol{P}}$, replace $P_{total}^{\boldsymbol{P}}$ with $P_{total'}^{\boldsymbol{P}}$ in Problem $\mathcal{S}_a^{\boldsymbol{P}}$ and start another iteration until reach the optimal results. And the proposed scheme for the positioning problem is summarized in Algorithm 3.

Algorithm 3 Proposed scheme for positioning process

Require : $\mathcal{S}^{\boldsymbol{P}}, \check{\mathcal{S}}^{\boldsymbol{P}}$

```
while B_total^P does not converge within max iterations do
    Node index: u = 0
    repeat
        u ⇐ u + 1
        B_u^P ← (31a),
    until u = U
    while P_total'^P does not converge within max iterations do
        repeat
            Reset: u = 0
            u ⇐ u + 1
            P_u^P ← (32a),
        until u = U
    end while
    Replace P_total^P with P_total'^P,
end while
return P_total'^P, B_u^P.
```

2) Communication process: Owing to *M* clusters for the communication process, the comprehensive problem could be decomposed into *M* clusters' sub-problem. Then $\mathscr{P}_3$ for *m*-th cluster reduce to

$$\mathscr{P}_4: \underset{\mathcal{S}_m^{\boldsymbol{C}} \ \mathcal{S}_m^{\boldsymbol{G}}}{\text{maximize}} \sum_{u=m_1}^{m_n} B_u^{\boldsymbol{C}} \log_2\left(1 + \mathrm{SNR}_u(P_u^{\boldsymbol{C}})\right) \tag{33}$$

$$\text{subject to}: \mathcal{S}_m^{\boldsymbol{C}} \subseteq \check{\mathcal{S}}_m^{\boldsymbol{C}},$$
$$\mathcal{S}_m^{\boldsymbol{G}} \subseteq \check{\mathcal{S}}_m^{\boldsymbol{G}}.$$

where $\mathcal{S}_m^{\boldsymbol{C}} \triangleq \left\{\mathcal{S}^{\boldsymbol{C}}\right\}_{u=m_1}^{m_n}$, $\mathcal{S}_m^{\boldsymbol{G}} \triangleq \left\{\mathcal{S}^{\boldsymbol{G}}\right\}_{u=m_1}^{m_n}$, and the constraint set are expressed similarly as $\check{\mathcal{S}}_m^{\boldsymbol{C}} \triangleq \left\{\check{\mathcal{S}}^{\boldsymbol{C}}\right\}_{u=m_1}^{m_n}$ and $\check{\mathcal{S}}_m^{\boldsymbol{G}} \triangleq \left\{\check{\mathcal{S}}^{\boldsymbol{G}}\right\}_{u=m_1}^{m_n}$.

Since Problem $\mathscr{P}_4$ is a mixed-integer problem, we could solve it with a modified GBD algorithm, in which the basic idea is to decompose the primal problem into two iterative sub-problem with strong constraints, as follows:

$$\mathscr{P}_{4,a}: \underset{\mathcal{S}_{m,a}^{\boldsymbol{C}}}{\text{maximize}} \sum_{u=m_1}^{m_n} B_u^{\boldsymbol{C}} \cdot \boldsymbol{\psi} \tag{34a}$$

$$\text{subject to}: \mathcal{S}_{m,a}^{\boldsymbol{C}} \subseteq \check{\mathcal{S}}_{m,a}^{\boldsymbol{C}}, \tag{34b}$$

$$\mathcal{S}_{m,a}^{\boldsymbol{G}} \subseteq \check{\mathcal{S}}_{m,a}^{\boldsymbol{G}}, \tag{34c}$$

$$\text{constraints on } \boldsymbol{\psi}, \tag{34d}$$

where $\mathcal{S}_{m,a}^{\boldsymbol{C}} \triangleq \mathcal{S}_m^{\boldsymbol{C}}\left\{R_u, B_u^{\boldsymbol{C}}\right\}$, $\mathcal{S}_{m,a}^{\boldsymbol{G}} \triangleq \left\{\mathcal{S}_{m,a}^{\boldsymbol{C}}, \mathcal{S}_m^{\boldsymbol{P}}\right\}$, and the constraint sets could be expressed similarly as $\check{\mathcal{S}}_{m,a}^{\boldsymbol{C}} \triangleq$

$\check{\mathcal{S}}_m^{\boldsymbol{C}}\{(21\text{c}),(21\text{d})\}$ and $\check{\mathcal{S}}_{m,a}^{\boldsymbol{G}} \triangleq \check{\mathcal{S}}_m^{\boldsymbol{G}}\{(23\text{b})\}$. It should be noted that the constraint (22a) denotes the lower bound of data rate so that the resource allocated for the positioning process should be considered again if Problem $\mathscr{P}_{4,a}$ has no optimal solution. And (34d) are constraints on $\boldsymbol{\psi}$ which come from $\mathscr{P}_{4,b}$ to cut the feasible solution space namely Benders cuts. In other words, in the initialization period, we utilize a slack variable $\boldsymbol{\psi}$ to represent $\log_2\left(1+\text{SNR}_u(P_u^{\boldsymbol{C}})\right)$, and the first constraint of (34d) would be the relaxed feasible region of $\boldsymbol{\psi}$. Then in the following iteration period, the feasible region of (34d) would be reduced according to the solution of Problem $\mathscr{P}_{4,b}$, as follows:

$$\mathscr{P}_{4,b}: \underset{\mathcal{S}_{m,b}^{\boldsymbol{C}}}{\text{maximize}}\ \boldsymbol{\psi} = \log_2\left(1+\text{SNR}_u(P_u^{\boldsymbol{C}})\right) \tag{35a}$$

$$\text{subject to}: \mathcal{S}_{m,b}^{\boldsymbol{C}} \subseteq \check{\mathcal{S}}_{m,b}^{\boldsymbol{C}}, \tag{35b}$$

$$\mathcal{S}_{m,b}^{\boldsymbol{G}} \subseteq \check{\mathcal{S}}_{m,b}^{\boldsymbol{G}}, \tag{35c}$$

where $\mathcal{S}_{m,b}^{\boldsymbol{C}} \triangleq \mathcal{S}_m^{\boldsymbol{C}}\left\{P_u^{\boldsymbol{C}}\right\}$, $\mathcal{S}_{m,b}^{\boldsymbol{G}} \triangleq \left\{\mathcal{S}_{m,b}^{\boldsymbol{C}}, \mathcal{S}_m^{\boldsymbol{P}}\right\}$, and the constraint sets could be expressed similarly as $\check{\mathcal{S}}_{m,b}^{\boldsymbol{C}} \triangleq \check{\mathcal{S}}_m^{\boldsymbol{C}}\{(21\text{b}),(21\text{d})\}$ and $\check{\mathcal{S}}_{m,b}^{\boldsymbol{G}} \triangleq \check{\mathcal{S}}_m^{\boldsymbol{G}}\{(23\text{a})\}$.

Algorithm 4 Proposed scheme for communication process

Require : $P_{total'}^{\boldsymbol{P}}, B_u^{\boldsymbol{P}}, M, \mathcal{S}_m^{\boldsymbol{C}}, \mathcal{S}_m^{\boldsymbol{G}}$ *and* $\varepsilon^{\boldsymbol{C}}$
Initialization : $LB = -\infty, UB = \infty$

```
Cluster index: m = 0
repeat
    m ⇐ m + 1
    while |UB − LB| > ε^C within max iterations do
        B_u^C ← (34a),
        ψ ← (36a)
        Update LB, UB,
    end while
    if |UB − LB| > ε^C then add constraints on (34d)
    end if
until m = M
return B_u^C and P_u^C for all user nodes.
```

In addition, $\mathscr{P}_{4,a}$ is the Master problem, and the objective function in (33) on the master problem's optimal solution denotes the lower bound of the primal problem, *LB*, while $\mathscr{P}_{4,b}$ is the Sub problem and its corresponding solution denotes the upper bound of the primal problem, *UB*.

In Problem $\mathscr{P}_{4,a}$, it is practicable to compute the solution owing to constraint (34d) and the distribution of channel gain. And the objective function of Problem $\mathscr{P}_{4,b}$ is Monotonically increasing, which means that Problem $\mathscr{P}_{4,b}$ could be transformed into seeking the maximize value of $\text{SNR}_u(P_u^{\boldsymbol{C}})$, as follows:

$$\mathscr{P}_{4,c}: \underset{\mathcal{S}_{m,b}^{\boldsymbol{C}}}{\text{maximize}}\ 2^{\boldsymbol{\psi}} - 1 = \text{SNR}_u(P_u^{\boldsymbol{C}}) \tag{36a}$$

$$\text{subject to}: \mathcal{S}_{m,b}^{\boldsymbol{C}} \subseteq \check{\mathcal{S}}_{m,b}^{\boldsymbol{C}}, \tag{36b}$$

$$\mathcal{S}_{m,b}^{\boldsymbol{G}} \subseteq \check{\mathcal{S}}_{m,b}^{\boldsymbol{G}}, \tag{36c}$$

Since Problem $\mathscr{P}_{4,c}$ is an univariate maximize programming with convex constraints, it could be efficiently solved by using the existing solver, e.g., the Simplex Method. By solving Problem $\mathscr{P}_{4,c}$, we could obtain the optimal value of $\boldsymbol{\psi}$. At this point, it is indispensable to examine whether this judgment condition is established or not, as follows:

$$|UB - LB| \leq \varepsilon^{\boldsymbol{C}} \tag{37}$$

where $\varepsilon^{\boldsymbol{C}}$ denotes the convergence tolerance parameter. And if (37) is satisfied, it means that Problem $\mathscr{P}_4$ has been solved and completed. The next step would be to calculate the communication problem for *M* clusters to acquire $B_u^{\boldsymbol{C}}$ and $P_u^{\boldsymbol{C}}$ for each user node. If not, (34d) would add another new constraint based on the solution of Problem $\mathscr{P}_{4,c}$. The comprehensive proposed solving scheme is summarized in Algorithm 4.

V. Simulation results

In this section, we present simulation results with the corresponding simulation settings listed in Table.I.

The center frequency and bandwidth are set to 38GHz and 200MHz, respectively. And the sub-carrier interval is set to 150MHz. Besides, the antenna arrays of the anchor nodes and user nodes are located at the same height of 1.5m. The anchor nodes use identical ULA which the inter-element distance between the antennas is set to 2.5mm. The user nodes utilize the same configuration, but the number of antennas is different. And N_t and N_r are set to 64 and 32 respectively. And the number of MPC is set to 1 to acquire the LoS dominant path.

TABLE I
SIMULTION PARAMETERS SETTINGS

Parameter	Configuration Value
Center Frequency	38GHz
Bandwidth	200MHz
Sub-carrier Interval	150kHz
Number of Anchor Node	4
Number of User Node	30
Antennas Number in Anchor Node	64
Antennas Number in User Node	32
SNR	10dB
Transmit Power	30-52dBm
Spectrum Density of Noise	-174dB/Hz
Number of MPC	1

As Fig.4 shows, the 4 known anchor nodes and 30 unknown user nodes are located at fixed positions in the two-dimensional $100m \times 100m$ area.

Fig.5 presents the clustering results for different cluster algorithms with the basis of the fixed locations of user nodes in Fig.4. And Fig.5(a) presents the final clusters with the LoS probability $\eta = 0.63$ by Algorithm 1 and Algorithm 2, while Fig.5(b) is formed with the LoS probability $\eta = 0.77$. Fig.5(c) and Fig.5(d) are formed with the same conditions by the AP algorithm and the K-means algorithm. And in Fig.5(d), there exist 6 known virtual CHs, which is the predetermined

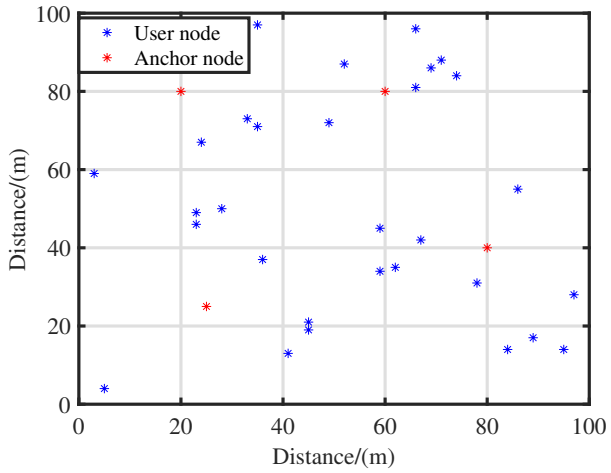

Fig. 4. Initial network geometry with 4 known anchor nodes and 30 unknown user nodes, and the four anchor nodes are located at (20,80), (25,25), (60,80), (80,40) respectively.

condition of the K-means algorithm. According to Fig.5(a) and Fig.5(b), there would be different cluster results with the change of η. Besides, there exists a Sole Cluster in Fig.5(b), which means the corresponding clustering results are improper. As for Fig.5(c), there would be 4 clusters which are less than 6 in Fig.5(a) and easier to suffer great interference between users. And for Fig.5(d), there would be 6 virtual CH in the topological network which is an additional cost for the systems where the cluster number also should be set in advance. In a word, Fig.5(a) presents the best clustering performance compared with other algorithms, and we adopt it as the clusters in the remaining simulation processes.

The goal of clustering algorithms is often to enhance "intra-cluster similarity and inter-cluster dissimilarity", so we define the ratio of the intra-cluster distance D_{in} to the inter-cluster distance D_{out} in (38) as the criterion to compare the effectiveness of different clustering algorithms, i.e., the Cluster Validity Index.

$$D = \frac{D_{\text{in}}}{D_{\text{out}}} = \frac{\sum_{a \in C_i} \sum_{k=1}^{K} \|a - c_k\|^2}{\sum_{k=1}^{K} \left\|c_k - \bar{C}\right\|^2} \tag{38}$$

where D_{in} denotes the sum of the distances from all cluster member nodes to their CHs, D_{out} denotes the sum of the distances from all CHs to the average of all CHs, K is the number of clusters, C_k denotes k-th cluster and c_k denotes the CH of C_k. $\bar{C}$ is the average of all CHs and a denotes the cluster member node.

Fig.6 indicates the Cluster Validity Index of three cluster algorithms including the proposed cluster algorithm with different η, the AP algorithm and the K-means algorithm with different number of user nodes. From the definition of the Cluster Validity Index and (38), it is obvious that a smaller value of D indicates a better clustering effect. In Fig.6, under the same number of user nodes, the clustering performance of the proposed algorithm is more effective than two traditional clustering algorithms and the performance with $\eta = 0.63$ outperforms that with $\eta = 0.77$ in theory. Because the clustering result of the proposed algorithm has the smaller intra-cluster distance and the greater inter-cluster distance compared with other algorithms as shown in Fig.5.

Fig.7 shows the contour plots of positioning performance metrics for various locations of a single user node within the topological network in Fig.4. In this simulation, the number of user nodes is set to 1 to acquire all locations' performance in the two-dimensional area. Since $U = 1$ and its changing location, there is no need to cluster for only one user, which means that all resources could be allocated to this user in the communication process or the positioning process. As for Fig.7(a), the PEB is increasing with the distance between the user node and anchor node adding, and the location of the anchor node has the lowest PEB. According to Fig.7(b), the distribution trend of OEB depends on the fixed location of anchor nodes, while the OEB is also lower in diagonal directions from each anchor node. On account of the formulation of PEB, it is proportional to the distance from the anchor node as Fig.7(a) shows. And for the OEB, the performance is also proportional to the distance from the anchor node.

Fig.8 presents the tradeoff between the sum rate and the PEB constraint in different resource allocation algorithms and different transmit power P_{total}. At first, it is clear that the proposed scheme performs always better than the average power algorithm in [44]. Then, as the PEB constraints are tighter, the sum rate improves at a peak value at first and then decreases to zero. Besides, both of the localization accuracy and the achievable sum rate could be higher when the transmit power improves. And the lower bound of PEB for the proposed scheme is also lower than the average power algorithm. As for the left part of the peak value, the sum rate increases when the PEB decreases. Because the channel estimation is imperfect at first, the channel estimation information would be more and more precise with the tighter PEB constraints. And the sum rate would reach the peak value when the channel estimation is perfect. As the right part of the peak value, there only exists competition between the communication and positioning process under the perfect channel estimation. Hence, the sum rate would decrease when the localization accuracy improves. And in Fig.8, we would acquire effective information about joint communication and position from the right part of the peak value.

Fig.9 presents the tradeoff between the sum rate and the PEB constraint in different resource allocation algorithms with different antennas numbers in anchor node N_t and antennas numbers in user node N_r. It is clear that the use of larger N_t and N_r can improve both of the localization accuracy and the achievable sum rate because the presence of antenna gain could promote communication and positioning performance simultaneously.

Fig.10 shows convergence behaviors of the proposed algorithms. Fig.10(a) shows the maximum cluster radius r_{max} and maximum transmission radius of nodes d^* within Algorithm 1 and Algorithm 2, that is, the proposed clustering algorithm. Fig.10(b) shows the value of $|UB - LB|$ in Algorithm 3 and Algorithm 4 within a few iterations, that is, the proposed resource allocation algorithm. As for Fig.10(a), the emergence of the inflection point means that there exists a Sole Cluster in

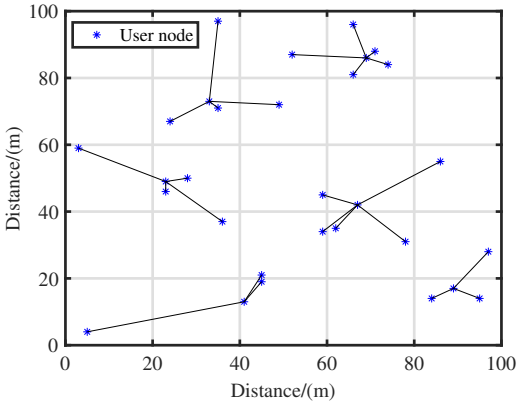

(a) Clusters with LoS probability $\eta = 0.63$ by the proposed clustering scheme.

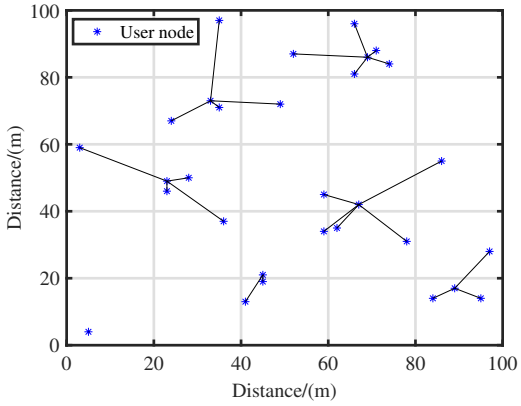

(b) Clusters with LoS probability $\eta = 0.77$ by the proposed clustering scheme.

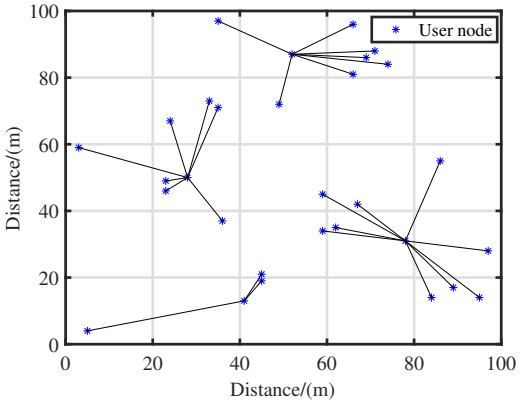

(c) Clusters by AP algorithm based on Euclidean distance.

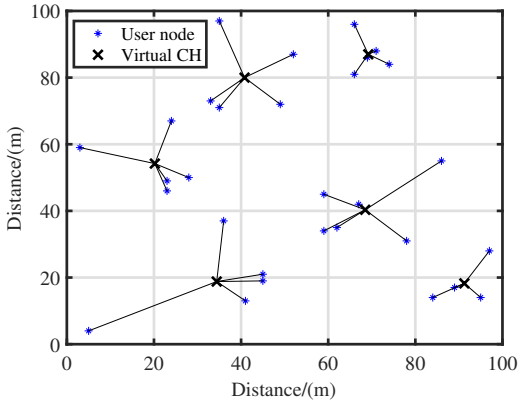

(d) Clusters by K-means algorithm with $K = 6$.

Fig. 5. Clustering results for different cluster algorithms within the fixed locations of user nodes.

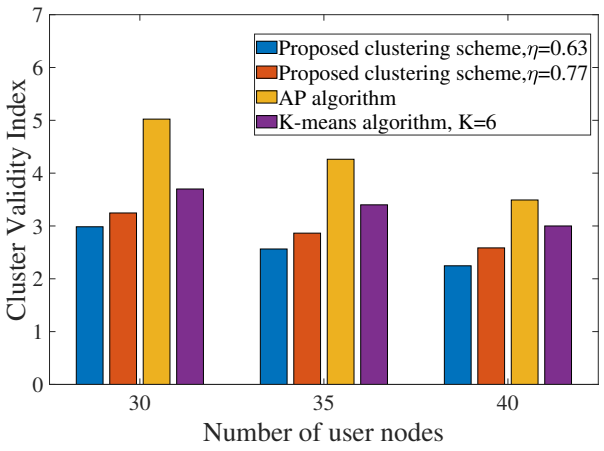

Fig. 6. Cluster Validity Index of different cluster algorithms with different number of user nodes.

the final clusters in this iteration. Hence, the LoS probability would be set afresh and continue the next iteration process. It is observed that the overall iteration time is related to the initial LoS probability. And for Fig.10(b), it proves that the proposed resource allocation has good convergence and high reliability.

VI. Conclusion

This paper has proposed a clustering scheme and resource allocation scheme in mmWave joint communication and positioning Ad hoc networks with F-OFDM. The user-centric design enables to premeditate the different degrees of demands for communication and positioning services, to guarantee the data rate and positioning accuracy for the user nodes by setting the same rate and accuracy constraints. In addition, the proposed clustering scheme supplies flexibility in the partition of the user nodes. Then the joint optimization of the positioning and communication process is realized by taking into account the LoS probability and distributing the remaining spectrum resources. It is shown that the proposed scheme could promote significantly the data rate and positioning accuracy performance by efficiently exploiting and allocating the wireless resources. From the results, we could conclude that mmWave Ad hoc networks can efficiently satisfy the users' demands of the communication process and positioning process with F-OFDM.

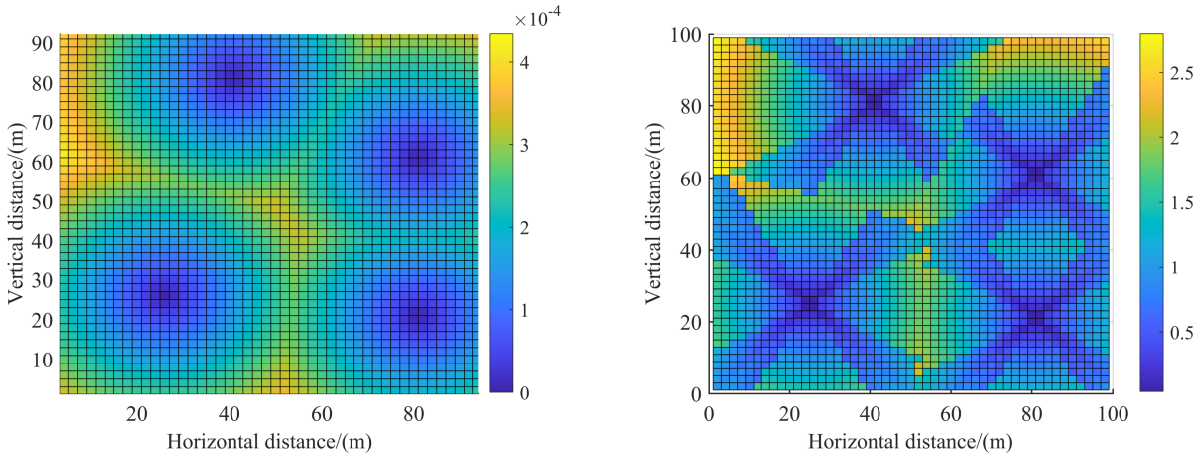

(a) PEB performance in the topological network.

(b) OEB performance in the topological network.

Fig. 7. Contour plots for different positioning performance metrics in the network and $P_{total}^{\boldsymbol{P}} = 30dBm$.

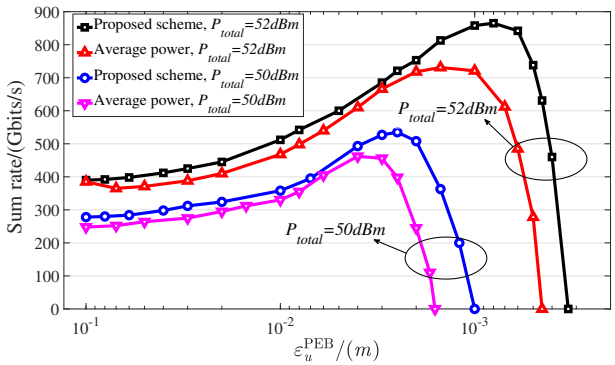

Fig. 8. Graph about sum rate and PEB constraint in different scheme with $P_{total} = 50dBm$ and $P_{total} = 52dBm$ respectively.

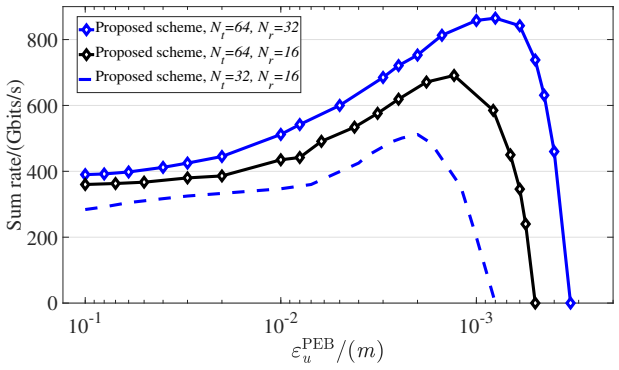

Fig. 9. Graph about sum rate and PEB constraint in proposed scheme with different N_t and N_r: $P_{total} = 52dBm$.

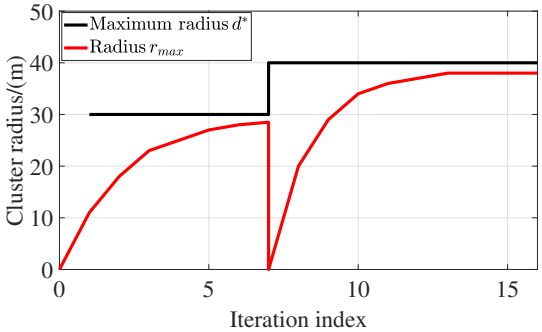

(a) The iteration graph of Algorithm 1 and Algorithm 2 jointly.

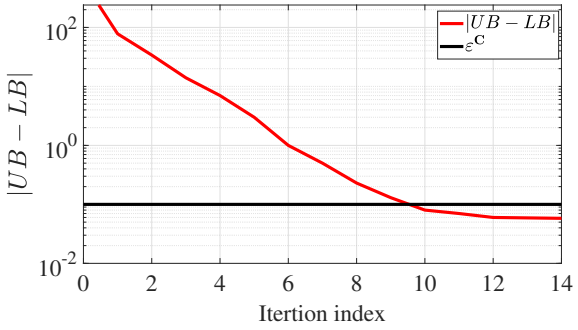

(b) The iteration graph of Algorithm 3 and Algorithm 4 jointly.

Fig. 10. Convergence behaviors of the proposed algorithms and $P_{total} = 50dBm$.

APPENDIX
DERIVATION OF FIM IN (9)

Combined (8) and (9) with (10), it is easy to derive a universal exemplar for matrix elements in $\boldsymbol{J}_{u,n}$, as expressed

$$\Phi\left(x_u, y_u\right) = \sum_{n=-N/2}^{N/2} \Phi_n\left(x_u, y_u\right) \tag{A.1}$$

where $\Phi\left(\cdot\right)$ are elements in $\boldsymbol{J}_u$, and $x_u, y_u = \left\{p_x^u, p_y^u, \alpha_u, H_u^R, H_u^I\right\}$. For the multiple sub-carrier case, we exploit the symmetry of beamformers and transmitted data considering $f_{-n} = f_n$ and $s_{-n} = s_n$ respectively to formulate the FIM as in (8). Besides, the relative direction angle α_u is equal to AoD θ_u in geometry so that the transmitted antenna array could be presented by $\boldsymbol{a}_u$ and $\dot{\boldsymbol{a}}_u = d\boldsymbol{a}_u/d\theta$. And d_u denotes the distance between user node and optimal anchor node in 2-Dimension.

Hence, the components of the FIM in $\boldsymbol{J}_u$, are as follows.

$$\begin{aligned}\Phi\left(p_x^u,p_x^u\right)&=4\pi^2\frac{B^2}{N^2}\left|h_u^2\right|d_{0,u}\boldsymbol{a}_u^{\mathrm{H}}\boldsymbol{X}_\tau\boldsymbol{a}_uA_1^2\\&+\left|h_u^2\right|d_{0,u}\dot{\boldsymbol{a}}_u^{\mathrm{H}}\boldsymbol{X}\dot{\boldsymbol{a}}_uA_2^2\\&+\left|h_u^2\right|d_{2,u}\boldsymbol{a}_u^{\mathrm{H}}\boldsymbol{X}\boldsymbol{a}_uA_3^2,\end{aligned}\tag{A.2a}$$

$$\begin{aligned}\Phi\left(p_x^u,p_y^u\right)&=4\pi^2\frac{B^2}{N^2}\left|h_u^2\right|d_{0,u}\boldsymbol{a}_u^{\mathrm{H}}\boldsymbol{X}_\tau\boldsymbol{a}_uA_1^2\\&-\left|h_u^2\right|d_{0,u}\dot{\boldsymbol{a}}_u^{\mathrm{H}}\boldsymbol{X}\dot{\boldsymbol{a}}_uA_2A_3\\&-\left|h_u^2\right|d_{2,u}\boldsymbol{a}_u^{\mathrm{H}}\boldsymbol{X}\boldsymbol{a}_uA_2A_3,\end{aligned}\tag{A.2b}$$

$$\Phi\left(p_x^u,\alpha_u\right)=\sqrt{\sigma_u}\left|h_u^2\right|d_{2,u}\boldsymbol{a}_u^{\mathrm{H}}\boldsymbol{X}a_uA_2,\tag{A.2c}$$

$$\Phi\left(p_x^u,H_u^R\right)=0,\tag{A.2d}$$

$$\Phi\left(p_x^u,H_u^I\right)=0,\tag{A.2e}$$

$$\begin{aligned}\Phi\left(p_y^u,p_x^u\right)&=4\pi^2\frac{B^2}{N^2}\left|h_u^2\right|d_{0,u}\boldsymbol{a}_u^{\mathrm{H}}\boldsymbol{X}_\tau\boldsymbol{a}_uA_1^2\\&-\left|h_u^2\right|d_{0,u}\dot{\boldsymbol{a}}_u^{\mathrm{H}}\boldsymbol{X}\dot{\boldsymbol{a}}_uA_2A_3\\&-\left|h_u^2\right|d_{2,u}\boldsymbol{a}_u^{\mathrm{H}}\boldsymbol{X}\boldsymbol{a}_uA_2A_3,\end{aligned}\tag{A.2f}$$

$$\begin{aligned}\Phi\left(p_y^u,p_y^u\right)&=4\pi^2\frac{B^2}{N^2}\left|h_u^2\right|d_{0,u}\boldsymbol{a}_u^{\mathrm{H}}\boldsymbol{X}_\tau\boldsymbol{a}_uA_1^2\\&-\left|h_u^2\right|d_{0,u}\dot{\boldsymbol{a}}_u^{\mathrm{H}}\boldsymbol{X}\dot{\boldsymbol{a}}_uA_3^2\\&+\left|h_u^2\right|d_{2,u}\boldsymbol{a}_u^{\mathrm{H}}\boldsymbol{X}\boldsymbol{a}_uA_3^2,\end{aligned}\tag{A.2g}$$

$$\Phi\left(p_y^u,\alpha_u\right)=-\sqrt{\sigma_u}\left|h_u^2\right|d_{2,u}\boldsymbol{a}_u^{\mathrm{H}}\boldsymbol{X}\boldsymbol{a}_uA_3,\tag{A.2h}$$

$$\Phi\left(p_y^u,H_u^R\right)=0,\tag{A.2i}$$

$$\Phi\left(p_y^u,H_u^I\right)=0,\tag{A.2j}$$

$$\Phi\left(\alpha_u,p_x^u\right)=\sqrt{\sigma_u}\left|h_u^2\right|d_{2,u}\boldsymbol{a}_u^{\mathrm{H}}\boldsymbol{X}\boldsymbol{a}_uA_2,\tag{A.2k}$$

$$\Phi\left(\alpha_u,p_y^u\right)=-\sqrt{\sigma_u}\left|h_u^2\right|d_{2,u}\boldsymbol{a}_u^{\mathrm{H}}\boldsymbol{X}\boldsymbol{a}_uA_3,\tag{A.2l}$$

$$\Phi\left(\alpha_u,\alpha_u\right)=\sigma_u\left|h_u\right|^2d_{2,u}\boldsymbol{a}_u^{\mathrm{H}}\boldsymbol{X}\boldsymbol{a}_u,\tag{A.2m}$$

$$\Phi\left(\alpha_u,H_u^R\right)=0,\tag{A.2n}$$

$$\Phi\left(\alpha_u,H_u^I\right)=0,\tag{A.2o}$$

$$\Phi\left(H_u^R,p_x^u\right)=0,\tag{A.2p}$$

$$\Phi\left(H_u^R,p_y^u\right)=0,\tag{A.2q}$$

$$\Phi\left(H_u^R,\alpha_u\right)=0,\tag{A.2r}$$

$$\Phi\left(H_u^R,H_u^R\right)=\sigma_ud_{0,u}\boldsymbol{a}_u^{\mathrm{H}}\boldsymbol{X}\boldsymbol{a}_u,\tag{A.2s}$$

$$\Phi\left(H_u^R,H_u^I\right)=0,\tag{A.2t}$$

$$\Phi\left(H_u^I,p_x^u\right)=0,\tag{A.2u}$$

$$\Phi\left(H_u^I,p_y^u\right)=0,\tag{A.2v}$$

$$\Phi\left(H_u^I,\alpha_u\right)=0,\tag{A.2w}$$

$$\Phi\left(H_u^I,H_u^R\right)=0,\tag{A.2x}$$

$$\Phi\left(H_u^I,H_u^I\right)=\sigma_ud_{0,u}\boldsymbol{a}_u^{\mathrm{H}}\boldsymbol{X}\boldsymbol{a}_u,\tag{A.2y}$$

where,

$$d_{0,u}=\left\|\boldsymbol{w}_u^{\mathrm{H}}\boldsymbol{a}_{R,u}\right\|_2^2,\tag{A.3}$$

$$d_{1,u}=\boldsymbol{a}_{R,u}\boldsymbol{w}_u^{\mathrm{H}}\frac{d}{d\alpha}\boldsymbol{w}_u^{\mathrm{H}}\boldsymbol{a}_{R,u},\tag{A.4}$$

$$d_{2,u}=\left\|\frac{d}{d\alpha}\boldsymbol{w}_u^{\mathrm{H}}\boldsymbol{a}_{R,u}\right\|_2^2,\tag{A.5}$$

$$\sigma_u=\frac{2P_uT_s\,\mathrm{Loss}_u}{N_0},\tag{A.6}$$

$$A_1=\sqrt{\sigma_u}\cos\left(\alpha_u\right)/c,\tag{A.7}$$

$$A_2=\sqrt{\sigma_u}\sin\left(\alpha_u\right)/d_u,\tag{A.8}$$

$$A_3=\sqrt{\sigma_u}\sin\left(\alpha_u\right)/d_u,\tag{A.9}$$

$$\boldsymbol{X}_\tau=\sum_{n=-N/2}^{N/2}\left|s_n\right|^2n^2\boldsymbol{F}_n,\tag{A.10}$$

$$\boldsymbol{X}=\sum_{n=-N/2}^{N/2}\left|s_n\right|^2\boldsymbol{F}_n.\tag{A.11}$$

And CRLB of variable μ_u could be expressed by $\boldsymbol{J}_u^{-1}$, which its first three diagonal elements are presented as follows

$$\begin{aligned}\boldsymbol{J}_{u,1,1}^{-1}&=Q\cdot\left\{4\pi^2\frac{B^2}{N^2}\left|h_u^2\right|d_{0,u}\boldsymbol{a}_u^{\mathrm{H}}X_\tau\boldsymbol{a}_uA_3^2\right\}^{-1}\\&+Q\cdot\left\{\left|h_u^2\right|d_{0,u}\dot{\boldsymbol{a}}_u^{\mathrm{H}}X\dot{\boldsymbol{a}}_uA_1^2\right\}^{-1},\end{aligned}\tag{A.12a}$$

$$\begin{aligned}\boldsymbol{J}_{u,2,2}^{-1}&=Q\cdot\left\{4\pi^2\frac{B^2}{N^2}\left|h_u^2\right|d_{0,u}\boldsymbol{a}_u^{\mathrm{H}}X_\tau\boldsymbol{a}_uA_2^2\right\}^{-1}\\&+Q\cdot\left\{\left|h_u^2\right|d_{0,u}\dot{\boldsymbol{a}}_u^{\mathrm{H}}X\dot{\boldsymbol{a}}_uA_1^2\right\}^{-1},\end{aligned}\tag{A.12b}$$

$$\boldsymbol{J}_{u,3,3}^{-1}=\left\{\sigma_u\left|h_u\right|^2d_{2,u}\boldsymbol{a}_u^{\mathrm{H}}X\boldsymbol{a}_u\right\}^{-1},\tag{A.12c}$$

with $Q=1/\left(A_1A_2+A_1A_3\right)$.

REFERENCES

[1] Y. Yao, F. Shu, Z. Li, X. Cheng, and L. Wu, "Secure transmission scheme based on joint radar and communication in mobile vehicular networks," *IEEE Transactions on Intelligent Transportation Systems*, 2023.

[2] S. G. Nagarajan, P. Zhang, and I. Nevat, "Geo-spatial location estimation for internet of things (iot) networks with one-way time-of-arrival via stochastic censoring," *IEEE Internet of Things Journal*, vol. 4, no. 1, pp. 205–214, 2017.

[3] H. Gao, B. Qiu, R. J. Duran Barroso, W. Hussain, Y. Xu, and X. Wang, "Tsmae: A novel anomaly detection approach for internet of things time series data using memory-augmented autoencoder," *IEEE Transactions on Network Science and Engineering*, pp. 1–1, 2022.

[4] Y. Gu, A. Lo, and I. Niemegeers, "A survey of indoor positioning systems for wireless personal networks," *IEEE Communications Surveys Tutorials*, vol. 11, no. 1, pp. 13–32, 2009.

[5] N. Tandon, B. Suman, N. Agarwal, and V. Bhatia, "Design and testability aspects of mobile adhoc networking waveform physical layer for software defined radio," in *2017 International Conference on Computing, Communication and Automation (ICCCA)*. IEEE, 2017, pp. 453–457.

[6] A. Thornburg and R. W. Heath, "Ergodic rate of millimeter wave ad hoc networks," *IEEE Transactions on Wireless Communications*, vol. 17, no. 2, pp. 914–926, 2018.

[7] H. Gao, C. Liu, Y. Yin, Y. Xu, and Y. Li, "A hybrid approach to trust node assessment and management for vanets cooperative data communication: Historical interaction perspective," *IEEE Transactions on Intelligent Transportation Systems*, pp. 1–10, 2021.

[8] K. A. Hamdi, "Precise interference analysis of ofdma time-asynchronous wireless ad-hoc networks," *IEEE Transactions on Wireless Communications*, vol. 9, no. 1, pp. 134–144, 2010.

[9] R. Singh, D. Saluja, and S. Kumar, "Reliability improvement in clustering-based vehicular ad-hoc network," *IEEE Communications Letters*, vol. 24, no. 6, pp. 1351–1355, 2020.

[10] S. H. Dokhanchi, B. S. Mysore, K. V. Mishra, and B. Ottersten, "A mmwave automotive joint radar-communications system," *IEEE Transactions on Aerospace and Electronic Systems*, vol. 55, no. 3, pp. 1241–1260, 2019.

[11] B. Ai, A. F. Molisch, M. Rupp, and Z.-D. Zhong, "5g key technologies for smart railways," *Proceedings of the IEEE*, vol. 108, no. 6, pp. 856–893, 2020.

[12] A. N. Uwaechia and N. M. Mahyuddin, "A comprehensive survey on millimeter wave communications for fifth-generation wireless networks: Feasibility and challenges," *IEEE Access*, vol. 8, pp. 62 367–62 414, 2020.

[13] A. Dogra, R. K. Jha, and S. Jain, "A survey on beyond 5g network with the advent of 6g: Architecture and emerging technologies," *IEEE Access*, vol. 9, pp. 67 512–67 547, 2021.

[14] Y. Li, H. Ma, L. Wang, S. Mao, and G. Wang, "Optimized content caching and user association for edge computing in densely deployed heterogeneous networks," *IEEE Transactions on Mobile Computing*, pp. 1–1, 2020.

[15] L. Yin, Q. Ni, and Z. Deng, "A gnss/5g integrated positioning methodology in d2d communication networks," *IEEE Journal on Selected Areas in Communications*, vol. 36, no. 2, pp. 351–362, 2018.

[16] A. Thornburg, T. Bai, and R. W. Heath, "Performance analysis of outdoor mmwave ad hoc networks," *IEEE Transactions on Signal Processing*, vol. 64, no. 15, pp. 4065–4079, 2016.

[17] Y. Zhu, L. Wang, K.-K. Wong, and R. W. Heath, "Secure communications in millimeter wave ad hoc networks," *IEEE Transactions on Wireless Communications*, vol. 16, no. 5, pp. 3205–3217, 2017.

[18] Y. Ding, S. Yan, X. Zhou, F. Shu, and S. Feng, "Radar-communication waveform design with detection probability constraints," *IEEE Wireless Communications Letters*, vol. 12, no. 1, pp. 168–172, 2023.

[19] G. Destino and H. Wymeersch, "On the trade-off between positioning and data rate for mm-wave communication," in *2017 IEEE International Conference on Communications Workshops (ICC Workshops)*. IEEE, 2017, pp. 797–802.

[20] G. Ghatak, R. Koirala, A. De Domenico, B. Denis, D. Dardari, B. Uguen, and M. Coupechoux, "Beamwidth optimization and resource partitioning scheme for localization assisted mm-wave communication," *IEEE Transactions on Communications*, vol. 69, no. 2, pp. 1358–1374, 2021.

[21] J. Saloranta, G. Destino, and H. Wymeersch, "Comparison of different beamtraining strategies from a rate-positioning trade-off perspective," in *2017 European Conference on Networks and Communications (EuCNC)*. IEEE, 2017, pp. 1–5.

[22] J. Saloranta and G. Destino, "Reconfiguration of 5g radio interface for positioning and communication," in *2017 25th European Signal Processing Conference (EUSIPCO)*. IEEE, 2017, pp. 898–902.

[23] L. Yin, J. Cao, K. Lin, Z. Deng, and Q. Ni, "A novel positioning-communication integrated signal in wireless communication systems," *Wireless Communications Letters, IEEE*, vol. 8, no. 5, pp. 1353–1356, 2019.

[24] L. Yin, J. Cao, T. Jiang, and Z. Deng, "Joint power allocation for a novel positioning-communication integrated signal," in *2020 IEEE/CIC International Conference on Communications in China (ICCC)*, 2020, pp. 923–928.

[25] R. Koirala, B. Denis, B. Uguen, D. Dardari, and H. Wymeersch, "Localization and communication resource budgeting for multi-user mm-wave mimo," in *2019 16th Workshop on Positioning, Navigation and Communications (WPNC)*. IEEE, 2019, pp. 1–5.

[26] X. Wang, P. Huang, J. Xie, and M. Li, "Ofdma-based channel-width adaptation in wireless mesh networks," *IEEE Transactions on Vehicular Technology*, vol. 63, no. 8, pp. 4039–4052, 2014.

[27] B. Farhang-Boroujeny, "Ofdm versus filter bank multicarrier," *IEEE Signal Processing Magazine*, vol. 28, no. 3, pp. 92–112, 2011.

[28] M. H. Mahmud, M. M. Hossain, A. A. Khan, S. Ahmed, M. A. Mahmud, and M. H. Islam, "Performance analysis of ofdm, w-ofdm and f-ofdm under rayleigh fading channel for 5g wireless communication," in *2020 3rd International Conference on Intelligent Sustainable Systems (ICISS)*, 2020, pp. 1172–1177.

[29] J. Abdoli, M. Jia, and J. Ma, "Filtered ofdm: A new waveform for future wireless systems," in *2015 IEEE 16th International Workshop on Signal Processing Advances in Wireless Communications (SPAWC)*, 2015, pp. 66–70.

[30] B. Yu, Y. Bao, K. Cheng, R. Chen, and X. Lu, "Resource virtualization and allocation for tdd-f-ofdm systems with mu-mimo," *IEEE Access*, vol. 8, pp. 219 047–219 061, 2020.

[31] G. Kwon, A. Conti, H. Park, and M. Z. Win, "Joint communication and localization in millimeter wave networks," *IEEE Journal of Selected Topics in Signal Processing*, vol. 15, no. 6, pp. 1439–1454, 2021.

[32] B. Soleimani and M. Sabbaghian, "Cluster-based resource allocation and user association in mmwave femtocell networks," *IEEE Transactions on Communications*, vol. 68, no. 3, pp. 1746–1759, 2020.

[33] A. Guerra, F. Guidi, and D. Dardari, "Single-anchor localization and orientation performance limits using massive arrays: Mimo vs. beamforming," *IEEE Transactions on Wireless Communications*, vol. 17, no. 8, pp. 5241–5255, 2018.

[34] M. K. Samimi, T. S. Rappaport, and G. R. MacCartney, "Probabilistic omnidirectional path loss models for millimeter-wave outdoor communications," *IEEE Wireless Communications Letters*, vol. 4, no. 4, pp. 357–360, 2015.

[35] S. Sun, T. S. Rappaport, T. A. Thomas, A. Ghosh, H. C. Nguyen, I. Z. Kovács, I. Rodriguez, O. Koymen, and A. Partyka, "Investigation of prediction accuracy, sensitivity, and parameter stability of large-scale propagation path loss models for 5g wireless communications," *IEEE Transactions on Vehicular Technology*, vol. 65, no. 5, pp. 2843–2860, 2016.

[36] A. Ghosh, T. A. Thomas, M. C. Cudak, R. Ratasuk, P. Moorut, F. W. Vook, T. S. Rappaport, G. R. MacCartney, S. Sun, and S. Nie, "Millimeter-wave enhanced local area systems: A high-data-rate approach for future wireless networks," *IEEE Journal on Selected Areas in Communications*, vol. 32, no. 6, pp. 1152–1163, 2014.

[37] M. Z. Win, Y. Shen, and W. Dai, "A theoretical foundation of network localization and navigation," *Proceedings of the IEEE*, vol. 106, no. 7, pp. 1136–1165, 2018.

[38] M. Z. Win, W. Dai, Y. Shen, G. Chrisikos, and H. Vincent Poor, "Network operation strategies for efficient localization and navigation," *Proceedings of the IEEE*, vol. 106, no. 7, pp. 1224–1254, 2018.

[39] A. Liu, Z. Huang, M. Li, Y. Wan, W. Li, T. X. Han, C. Liu, R. Du, D. K. P. Tan, J. Lu *et al.*, "A survey on fundamental limits of integrated sensing and communication," *IEEE Communications Surveys & Tutorials*, vol. 24, no. 2, pp. 994–1034, 2022.

[40] R. Koirala, B. Denis, B. Uguen, D. Dardari, and H. Wymeersch, "Localization and throughput trade-off in a multi-user multi-carrier mm-wave system," *IEEE Access*, vol. 7, pp. 167 099–167 112, 2019.

[41] Y. Shen and M. Z. Win, "Fundamental limits of wideband localization—part i: A general framework," *IEEE Transactions on Information Theory*, vol. 56, no. 10, pp. 4956–4980, 2010.

[42] H. Gao, J. Xiao, Y. Yin, T. Liu, and J. Shi, "A mutually supervised graph attention network for few-shot segmentation: The perspective of fully utilizing limited samples," *IEEE Transactions on Neural Networks and Learning Systems*, pp. 1–13, 2022.

[43] Frey, J. Brendan, Dueck, and Detbert, "Clustering by passing messages between data points." *Science*, 2007.

[44] V. Hindumathi and K. Ramalingareddy, "Improvement of efficiency of mimo-ofdm system using channel adaptive subcarriers allocation algorithm with equal power," in *2016 International Conference on Inventive Computation Technologies (ICICT)*, vol. 3, 2016, pp. 1–6.

Xueni Luo was born in Hunan, China. She received the B.Sc. degree in communication engineering from Xidian University, Xi'an, China, in 2021. She is currently pursuing the M.Sc. degree in communication and information system with the State Key Laboratory of Integrated Service Networks, Xidian University, Xi'an. Her research interests include OFDM, mmWave, and resource allocation of wireless communications.

Xiaofeng Lu received the B.Sc. degree from Sichuan University, Chengdu, China, in 1996, the M.Sc. degree from Hunan University, Changsha, China, in 1999, and the Ph.D. degree from the Huazhong University of Science and Technology, Wuhan, China, in 2006. From 1999 to 2003, he was a Research and Development Engineer with the Wuhan Research Institute of Post and Telecommunications. He is currently a Full Professor with the State Key Laboratory of Integrated Service Networks, Xidian University, Xi'an, China. His main research interests include broadband wireless communications, signal processing, resource allocation, MU-MIMO, joint communication and localization and OFDMA.

Benquan Yin was born in Anhui, China. He received the B.Sc. degree in optoelectronic information science and technology from Xidian University, Xi'an, China, in 2020. He is currently pursuing the M.Sc. degree in communication and information system with the State Key Laboratory of Integrated Service Networks, Xidian University, Xi'an, China. His research interests include millimeter wave, virtual MIMO, and resource allocation of wireless communications.

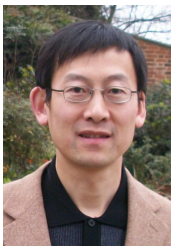

Kun Yang (Fellow, IEEE) received his PhD from the Department of Electronic and Electrical Engineering of University College London (UCL), UK, and MSc and BSc from the Computer Science Department of Jilin University, China. He is currently a full Professor in the School of Computer Science and Electronic Engineering, University of Essex, UK. Before joining in University of Essex at 2003, he worked at UCL on several European Union (EU) research projects for several years. His main research interests include heterogeneous wireless networks, fixed mobile convergence, future Internet technology and network virtualization, cloud computing. He has published 60+ journal papers. He serves on the editorial boards of both IEEE and non-IEEE journals.